Neuronal Ablation of IKK2 Decreases Lesion Size and Improves Functional Outcome after Spinal Cord Injury in Mice

Ellman, Ditte Gry; Novrup, Hans Gram ; Jørgensen, Louise Helskov; Lund, Minna Christiansen; Yli-Karjanmaa, Minna Liisa Kyllikki; Madsen, Pernille Marie; Vienhues, Jonas Heinrich; Dursun, Safinaz; Bethea, John R.; Lykke-Hartmann, Karin; Brambilla, Roberta; Lambertsen, Kate Lykke

Published in:
JSM Neurosurgery and Spine

Publication date:
2017

Document version
Publisher's PDF, also known as Version of record

Document license
CC BY

Citation for pulished version (APA):
Ellman, D. G., Novrup, H. G., Jørgensen, L. H., Lund, M. C., Yli-Karjanmaa, M. L. K., Madsen, P. M., ... Lambertsen, K. L. (2017). Neuronal Ablation of IKK2 Decreases Lesion Size and Improves Functional Outcome after Spinal Cord Injury in Mice. JSM Neurosurgery and Spine, 5(3), [1090].

SciMedCentral

JSM Neurosurgery and Spine

Research Article

Neuronal Ablation of IKK2 Decreases Lesion Size and Improves Functional Outcome after Spinal Cord Injury in Mice

Ditte Gry Ellman[1], Hans Gram Novrup[1], Louise Helskov Jørgensen[2], Minna Christiansen Lund[1], Minna Yli-Karjanmaa[1], Pernille Marie Madsen[1,3], Jonas Heinrich Vienhues[1], Safinaz Dursun[1], John R. Bethea[3,4], Karin Lykke-Hartmann[5], Roberta Brambilla[3], and Kate Lykke Lambertsen[1,6,7]*

[1]*Neurobiology Research, University of Southern Denmark, Denmark*
[2]*Department of Pathology, Odense University Hospital, Denmark*
[3]*The Miami Project to Cure Paralysis, University of Miami Miller School of Medicine, USA*
[4]*Department of Biology, Drexel University, USA*
[5]*Department of Biomedicine, Aarhus University, Denmark*
[6]*Department of Neurology, Odense University Hospital, Denmark*
[7]*Department of Clinical Research, University of Southern Denmark, Denmark*

***Corresponding author**
Kate Lykke Lambertsen, Department of Neurology, Odense University Hospital, Denmark, J.B. Winsloewsvej 21, st, DK-5000 Odense C, Denmark, Tel: 4565503806; Email: klambertsen@health.sdu.dk

Submitted: 11 July 2017

Accepted: 08 August 2017

Published: 10 August 2017

Keywords

- Nuclear factor-kappa B
- Spinal cord injury
- Neurons
- Functional outcome

Abstract

Nuclear factor-kappa B (NF-κB) is a key modulator of inflammation and secondary injury responses in neurodegenerative disease, including spinal cord injury (SCI). Inhibition of astroglial NF-κB reduces inflammation, enhances oligodendrogenesis and improves functional recovery after SCI, however the contribution of neuronal NF-κB to secondary inflammatory responses following SCI has yet to be investigated. We demonstrate that conditional ablation of IKK2 in Synapsin 1-expressing neurons in mice (Syn1creIKK2$^{fl/fl}$) reduces activation of the classical NF-κB signaling pathway, resulting in impaired motor function and altered memory retention under naïve conditions. Following induction of a moderate SCI phosphorylated NF-κB levels decreased in the spinal cord of Syn1creIKK2$^{fl/fl}$ mice compared to controls, resulting in improvement in functional recovery. Histologically, Syn1creIKK2$^{fl/fl}$ mice exhibited reduced lesion volume but comparable microglial/leukocyte responses after SCI. In parallel, interleukin (IL)-1β expression was significantly decreased within the lesioned spinal cord, whereas IL-5, IL-6, IL-10, tumor necrosis factor (TNF) and chemokine (C-X-C motif) ligand 1 were unchanged compared to control mice. We conclude that conditional ablation of IKK2 in neurons, resulting in reduced neuronal NF-B signaling, and lead to protective effects after SCI and propose the neuronal classical NF-κB pathway as a potential target for the development of new therapeutic, neuroprotective strategies for SCI.

ABBREVIATIONS

ASF: Area Sampling Fraction; BMS: Basso Mouse Scale; DAB: Diaminobenzidine; EAE: Experimental Autoimmune Encephalomyelitis; EM: Electron Microscopy; EPM: Elevated Plus Maze; EtOH: Ethanol; FBS: Foetal Bovine Serum; GFAP: Glial Fibrillary Acidic Protein; H&E: Hematoxylin and Eosin; HRP: Horse-Radish Peroxidase; IKK: IκB kinase; iNOS: Inducible Nitric Oxide Synthase; IL: Interleukin; IL-1Ra: Interleukin-1 Receptor Antagonist; LFB: Luxol Fast Blue; NF-κB: Nuclear Factor-Kappa B; PBS: Phosphate-Buffered Saline; PFA: Paraformaldehyde; RM: Repeated Measures; SCI: Spinal Cord Injury; SAB: Spontaneous Alternation Behavior; SDU: University of Southern Denmark; SSF: Sampling Section Fraction; Syn1: Synapsin 1; TB: *Toluidine Blue*; TBS: Tris-Buffered Saline; TBS+T: TBS Containing 0.1% Triton; TEG: Triethylene Glycol; TNF: Tumor Necrosis Factor; TSF: Thickness Sampling Fraction; UM: University of Miami

INTRODUCTION

The nuclear factor-kappa B (NF-κB) transcription factor plays an important role in regulation of the immune and inflammatory processes. Neuronal and glial activation of NF-κB has been implicated in the pathophysiological changes following traumatic spinal cord injury (SCI) [1-5]. NF-κB is known to regulate the synthesis of numerous genes involved in secondary injury mechanisms, such as glial- and neuronal-derived chemokines (e.g. CCL2, CCL5, CXCL1) and cytokines (e.g. tumor necrosis factor (TNF), interleukin (IL)-1) [6,7]. Furthermore, inhibition of NF-κB results in reduced infiltration of inflammatory cells [8,9] and increased oligodendrogenesis after SCI [3], which have been linked to Neuroprotection.

In non-stimulated cells, NF-κB dimers are maintained in the cytosol through binding with the inhibitory proteins IBs (e.g. IκB,, and). In response to cell stimulation (e.g. cytokines, glutamate,

oxidative damage), the IκB kinase (IKK) complex consisting of the IKK1 and IKK2 catalytic subunits and the NEMO regulatory protein [10], is rapidly activated resulting in phosphorylation of the regulatory domain of the IκBs. This signals to the degradation of IB, releasing activated NF-κB to translocate to the nucleus and initiate transcription. IKK2 and NEMO are required for NF-κB activation through the "canonical" pathway involving degradation of IκBα, while IKK1 mediates NF-κB activation through the "alternative" pathway [11].

NF-κB, IKK2 and NEMO deficient mice in all neuroectodermal cells have shown suppressed or ameliorated disease following experimental autoimmune encephalomyelitis (EAE) [12,13], suggesting that targeting of the IKK-NF-κB pathway could be therapeutic. However, as NF-κB activity was inhibited in all neuroectodermal cells in these studies, these experimental settings do not allow evaluation of the function of NF-κB in specific cells of the CNS. In addition, Brambilla et al., have shown that astroglial NF-κB inhibition is therapeutic in EAE [9,14]. Studies based on the use of mice where NF-κB was functionally inactivated selectively in astrocytes have shown that these transgenic mice display improved functional recovery compared to littermates following SCI [2,5] and that oligodendrogenesis is improved when astroglial NF-κB is inhibited [3]. In comparison, selective neuronal inhibition of NF-κB, was shown to reduce infarct size in a model of focal cerebral ischemia [15], demonstrating that neuronal NF-κB activation can contribute to brain damage. In the present study, we investigated the effect of conditional IKK2 ablation in Synapsin 1-expressing neurons on behavior under naïve conditions and functional outcome, lesion volume and neuroinflammation after moderate SCI.

MATERIALS AND METHODS

Mice

Experiments were performed according to protocols approved by The Danish Animal Inspectorate under the Ministry of Food and Agriculture (J. No. 2008-561-1523 and 2013-15-2934-00924) and according to guidelines approved by the Institutional Animal Care and Use Committee of the University of Miami. Syn1CreIKK2$^{fl/fl}$ transgenic breeders were transferred from UM to the Biomedical Laboratory, SDU, where they were maintained as a breeding colony. These mice were originally generated by crossing Synapsin 1 promoter driven Cre (Syn1cre) transgenic mice [16] with IKK2$^{fl/fl}$ mice [17]. All mice were 2-4 months old females and littermate (IKK2$^{fl/fl}$) mice were used as controls. Animals were housed under diurnal lightning conditions in a virus/antigen free facility free access to water and food.

Genotyping

DNA was extracted from tail biopsies from 3-4 weeks old mice using the NucleoSpin Tissue kit (Macherey-Nagel) according to the manufacturer's protocol. Syn1cre primers: forward 5'-GCGGTCTGGCAGTAAAAACTATC and reverse 5'GTGAAACAGCATTGCTGTCACTT. IKK2 primers: forward 5'-CCTTGTCCTATAGAAGCACAA and reverse 5'-GTCATTTCCACAGCCCTG (DNA Technology). PCR products were visualized using the FlashGel system (Lonza).

Tissue processing

Mice were deeply anaesthetized using an overdose of pentobarbital (200 mg/ml) containing lidocaine (20 mg/ml) and perfused through the left ventricle with cold 4% paraformaldehyde (PFA) in phosphate-buffered saline (PBS).

Toluidine blue (TB) staining and electron microscopy (EM) analyses: For EM and TB analyses of axons and myelin, 1 mm segments of the thoracic spinal cords were processed as previously described [9]. One μm thick sections were obtained with a Leica Ultracut E microtome and stained with 1% TB solution.

Paraffin histopathology and immunohistochemical analysis: Spinal cords were removed and tissue segments containing the lesion area were paraffin-embedded and cut into 10 parallel series of 15μm thick microtome sections. Furthermore, in naïve mice lung, heart, liver, diaphragm, spleen, the anterior tibialis muscle and small intestine biopsies were imbedded in paraffin and cut into 5μm thick sections. Sections were then stained using Hematoxylin and Eosin (H&E) [3]. For stereological analysis of the total number of astrocytes in the hilus of the hippocampus, brains were processed as previously described [18] and cut horizontally into six 60μm-thick parallel series of free floating vibratome sections and cryo-protected in de Olmo's solution.

Estimation of myelinated axons

The number of TB-stained myelinated axons was estimated at 60X magnification using the VisioMorph software (VisioPharm) applying a 200x200μm sampling grid and a 25x25μm counting frame. From the same specimens, ultra-thin sections (60-90 nm-thick) were cut for EM assessments (see below).

Quantification of g-ratios

For evaluation of the g-ratio (axonal diameter/fiber diameter) of axons in the thoracic spinal cord, EM micrographs were taken at a magnification of 5.2K (Phillips CM-10 transmission electron microscope). A grid was placed over the section and pictures taken randomly from each quadrant corresponding to the lateral columns of the cord. One picture per quadrant was evaluated for a minimum of 12 images/mouse. On each micrograph, fiber diameter and axon diameter of each axon were measured with the aid of Image J software, as previously described [9].

Behavioral tests

Barnes maze: Barnes maze was administered to assess cognitive function in learning and memory of naïve Syn1creIKK2$^{fl/fl}$ and IKK2$^{fl/fl}$ mice using a modified protocol described by Attar et al. [19]. All sessions were recorded using a SONY HDR-CX240E camera.

Mice interacted with the Barnes maze in three phases: habituation (1 day), training (3 days), and probe (1 day). They were housed in the behavior room during the whole experiment. Before starting each experiment, mice were placed in individual holding cages where they remained until the end of their testing sessions.

On the habituation day, mice were placed in the center of the maze inside a transparent starting cylinder (diameter: 8

cm; height: 12.5 cm) for 30 sec. Then mice were guided slowly by moving the cylinder towards the target hole that lead to the escape box while loud heavy metal music was played. After 10-15 sec the cylinder was removed and mice were given 3 min to independently enter through the target hole into the escape box. If they did not enter on their own during that time, they were gently guided. Mice were allowed to stay in the escape box for 1 min with the music turned off before being returned to the holding cage.

In the training phase, mice were placed inside a non-transparent starting cylinder placed in the center of the maze for 15 sec. At the end of the holding period, the music was started, a buzzer turned on, and they were allowed to explore the maze for 3 min. If a mouse found the escape box and entered it during that time, it was allowed to stay there for 1 min. If it did not find the escape box, it was gently guided towards it. The buzzer was turned off once the mouse entered the escape box and the music was stopped. This was done with 6 mice at a time, providing 20-30 min inter-trial interval. The total number of trials each day was 5.

On the probe day, the escape box was removed and the mice were placed inside the starting cylinder placed in the center of the maze for 15 sec, the buzzer and the music were turned on, and the cylinder removed. Each mouse was given 2 min to explore the maze, at the end the buzzer and the music were turned off and the mouse was returned to its holding cage. After the first 4 trials, external cues were exchanged 180° and the test was repeated, in order to test whether the mouse used external clues to navigate after. Measures of time spent in the quadrant where the escape box used to be (target quadrant) were recorded, along with time spent in the positive, negative and opposite quadrants. For these analyses, the maze was divided into quadrants of 5 holes.

Y-maze test

Spontaneous alternation behavior (SAB) and hence working memory was tested using the Y-maze test in naïve mice as previously described [20]. Each mouse was placed in the arm designated (A). Except for the first two, the number of entries into each arm (A-C) was recorded manually over an 8 min period and spontaneous alternation calculated based on these numbers.

Open field test

The open field test was performed as previously described [21]. The distance travelled (m), speed (cm/sec) and the entries into the three zones (wall, inter periphery and center of the box) were recorded automatically. Rearing, grooming, digging, urination and droppings were recorded manually and are presented as number (n) of events.

Elevated plus maze test

To further examine anxiety-like behavior, naïve mice were subjected to the elevated plus maze. The elevated plus maze (EPM) apparatus consisted of two open arms and two closed arms (30cm x 5cm). The entire maze was elevated 40cm from the floor. Each mouse was placed in the center of the maze with the head facing towards the open arm. During a 5 min test, the time spent in the closed and open arms and the total distance moved were recorded using the SMART video tracking software.

Grip strength

The grip strength meter (BIO-GT-3, BIOSEB) was used to study neuromuscular function in naïve mice as previously described [22].

Rotarod performance

In order to evaluate motor coordination/performance and balance in naïve conditions, we performed the rotarod test as previously described [18,22].

Basso Mouse Scale

Functional recovery of loco motor function after SCI was determined by scoring of the hindlimb performance in the open field using the Basso Mouse Scale (BMS) system, a 0 to 9 rating system designed specifically for the mouse [21,23]. Only mice with a score below 2 on day 1 were included.

Thermal hyperalgesia

Thermal hyperalgesia was tested with a Hargreave's heat source by using the Plantar Test apparatus (Ugo Basile), as previously described [21]. The behavioral test was performed before SCI and once a week on each animal if and when they reached a BMS score of 5.

Rung Walk

In order to test stepping, interlimb coordination and balance, mice were tested on the rung walk if and when they reached a BMS score of 5, as previously described [21].

INDUCTION OF SPINAL CORD INJURY

Mice were anaesthetized using a ketamine (100 mg/kg, VEDCO Inc)/xylazine (10 mg/kg, VEDCO Inc) cocktail, laminectomized between vertebrae T8 and T10, and the impactor induced an approximate displacement of 500 μm (moderate injury) [21]. Following SCI mice were injected with saline to prevent dehydration and buprenorphine hydrochloride (0.001 mg/20 g Temgesic) four times at eight-hour intervals, starting immediately after surgery. Mice were housed separately in a recovery room, where their post-surgical health status was monitored during a 24-48 hour. Manual bladder expression was performed twice a day. Body weight was monitored weekly. In addition, mice received s.c. prophylactic injections of antibiotic gentamicin (40 mg/kg) for 7 days to prevent urinary tract infections.

HISTOLOGY

Klüver-Barrera Luxol Fast Blue (LFB) staining for myelinated fibers

For evaluation of lesion pathology, sections were stained in 0.1% LFB at 60°C overnight as previously described [24].

H&E staining

Muscle (heart and anterior tibialis), spleen, liver, small intestine and lung tissue was stained with H&E according to standard protocols at the Department of Pathology, Odense University Hospital [25].

Immunohistochemistry and immunofluorescence staining

7.3.1. CD45 and F4/80 immunohistochemical staining: Staining for CD45 (1:100; 30-F11 (Ly 5), BD Pharmingen) or F4/80 (1:100; AbDSerotec) for microglia/macrophages was performed on spinal cord tissue from mice with 35 days survival after SCI (CD45 and F4/80) and on heart, tibialis, and diaphragm musculature from naïve mice (CD45) as previously described [24].

NeuN staining for estimation of the number of neurons in the spinal cord in naïve conditions: Sections were deparaffinized and rehydrated in xylene, 99% EtOH, 96% EtOH, 70% EtOH, followed by running tap water. The sections were demasked in triethylene glycol (TEG)-buffer using a steamer, cooled at room temperature before rinsing in running tap water, followed by dH_2O. Next, sections were rinsed in TBS, blocked in methanol containing H_2O_2 and briefly rinsed in TBS, followed by TBS containing 0.1 % triton (TBS+T). Next, sections were pre-incubated with 10% fetal bovine serum (FBS) in TBS and incubated with biotinylated anti-NeuN antibody (1:500; Millipore) overnight at 4°C. The sections were hereafter incubated with HRP-conjugated Streptavidin (1:200; Amersham) and developed using diaminobenzidin (DAB) dissolved in TBS containing hydrogen peroxide. Sections were counter stained with TB and mounted with Depex.

Glial fibrillary acidic protein (GFAP) staining for estimation of the number of astrocytes: Free-floating brain sections was blocked for endogenous peroxidase activity using methanol and peroxide in TBS, then incubated with 10% FBS in 0.05M TBS+T. Sections were incubated with anti-GFAP primary antibody (1:1,200; DakoCytomation) at 4°C, followed by biotinylated anti-rabbit secondary antibody (GE Healthcare) diluted 1:200 in TBS+T at room temperature. Sections were rinsed with TBS+T, incubated with HRP-conjugated streptavidin (1:200; GE Healthcare) and developed using DAB and hydrogen peroxide diluted in TBS. Finally, sections were transferred to gelatin-coated glass slides, counter-stained with TB, dehydrated and mounted with Depex [18].

Quantification of neurons and astrocytes

Estimation of the number of NeuN$^+$ neurons in the spinal cord in naïve conditions: The number of neurons was counted in the grey matter in the thoracic part of the spinal cord by systematic uniform random sampling with the following parameters: x-step = 200 µm and y-step = 200, and stepping area = 5,625 µm^2 on the VisioMorph platform (VisioPharm). Every tenth section was counted in a 480 µm long piece of the thoracic spinal cord. The total number of NeuN$^+$ neurons (N) was estimated as using the formula: Estimate of N = ∑Q Ŋ (1/ssf) Ŋ (1/asf) Ŋ (1/tsf), where 1/tsf was the thickness sampling fraction (1/tsf = 1), 1/ssf is the sampling section fraction (1/ssf = 10), and 1/asf is the area sampling fraction (40,000/5,625) as previously described [21]. Estimates are presented as number of NeuN$^+$ neurons/480 µm of spinal cord.

Estimation of the number of GFAP$^+$ astrocytes in naïve conditions: The total number of GFAP$^+$ astrocytes was estimated in the hilus of the dentate gyrus in the hippocampus using a x-step of 65.94 µm and a y-step of 65.94 µm, and a stepping area of 5,000 µm^2 on the VisioMorph platform [18]. Estimates are presented as total number of GFAP$^+$ astrocytes/mm^2.

Lesion volume estimation

The volume of the injury was determined from the area of every tenth section sampled by systematic uniform random sampling. The area of the lesion site was estimated as previously described [21,24,25] using the VisioMorph software and Cavalieri's principle for volume estimation.

Protein purification

Cytosolic and nuclear protein extracts from naïve mice and mice exposed to SCI and allowed to survive for 3 days were purified from 1 cm thoracic spinal cord tissue (naïve conditions) or 1 cm spinal cord tissue centered on the lesion, respectively. The samples were lysed in Complete Mesoscale Lysis Buffer and tip-sonicated, followed by centrifugation at 1,000 g at 4°C. The supernatants were collected and centrifuged at 5,500 g at 4°C. Supernatants, containing the cytosolic and smaller membrane fragments, were collected and stored at -80°C. Pellets were washed twice with Complete Mesoscale Lysis Buffer, including centrifugations at 1,000 g at 4°C. Finally, the nuclear fraction, were dissolved in Completed Mesoscale Lysis Buffer and stored at -80°C. Protein concentrations were determined using the Pierce BCA Protein Assay Kit (Thermo Scientific) according to the manufacturer's protocol.

Nuclear factor-kappa B (NF-κB) analysis

Quantitative determination of nuclear and cytoplasmic phosphorylated NF-κB (Ser536) was investigated in mice with 3 days survival after SCI using the phospho-NFκB (Ser536) whole cell lysate kit from Mesoscale, according to the manufacturer's instructions. Data was analyzed using MSD Discovery Workbench software [26,27].

Multiplex analysis

Cytokine expression was estimated in naïve mice and in mice with 3 days survival after SCI using the MSD Mouse Proinflammatory V-Plex Plus Kit from Mesoscale and a SECTOR Imager 6000 (Mesoscale Discovery) Plate Reader according to the manufacturer's instructions [18,27]. Data was analyzed using MSD Discovery Workbench software.

ELISA

IL-1Ra expression was estimated in naïve mice and mice with 3 days survival after SCI using ELISA (MRA00, R&D) as previously described [28]. Measurements were normalized to the total protein content of the sample as measured using the method by Bradford [29].

Statistical analysis

Comparisons were performed using repeated measures (RM) two-way ANOVA followed by multiple t-test analysis, by two-way ANOVA followed by the appropriate *post-hoc* test or by Student's t-test. Linear correlation analysis between cytokines 3 days after SCI was performed using Pearson correlation test. The g-ratio

data were analyzed by linear regression, and slope and elevation parameters were used to compare groups. Analyses were performed using Prism 4.0b software for Macintosh, (GraphPad Software). Data are presented as mean ± SEM. Statistical significance was established for $p<0.05$.

RESULTS

Phenotypic characterization of Syn1creIKK2$^{fl/fl}$ mice

Prior to addressing the effect of neuronal ablation of IKK2 on lesion size and functional recovery after SCI, we characterized the Syn1creIKK2$^{fl/fl}$ mice along with their littermates (IKK2$^{fl/fl}$) under naïve conditions.

Syn1creIKK2$^{fl/fl}$ mice bred normally and had a normal physical appearance (Supplemental Figure 1A, B). However, body weight of adult Syn1creIKK2$^{fl/fl}$ mice (21.37 ± 0.36 g, n=15) was significantly increased compared to littermates (20.17 ± 0.39 g, n=19) ($p<0.05$). This, together with previous findings of shifted muscle fiber distribution and improved muscle force in mice with muscle-restricted NF-κB signaling in creatine kinase^{+} cells [30] led us to investigate whether there was any abnormal muscle phenotype in Syn1creIKK2$^{fl/fl}$ mice. When examining the anterior tibialis and the diaphragm muscles using H&E staining (Supplemental Figure 1C) and anti-CD45 for infiltrating immune cells (Supplemental Figure 1D), we did not observe any abnormal phenotype in Syn1creIKK2$^{fl/fl}$ mice compared to littermates, indicating no difference in the inflammatory states. Heart, spleen, liver, small intestine and lungs did not show any morphological abnormality as well (Supplemental Figure 1C,D,E).

Neuronal ablation of IKK2 affects g-ratio

Lack of neuronal NF-κB signaling did not result in changes

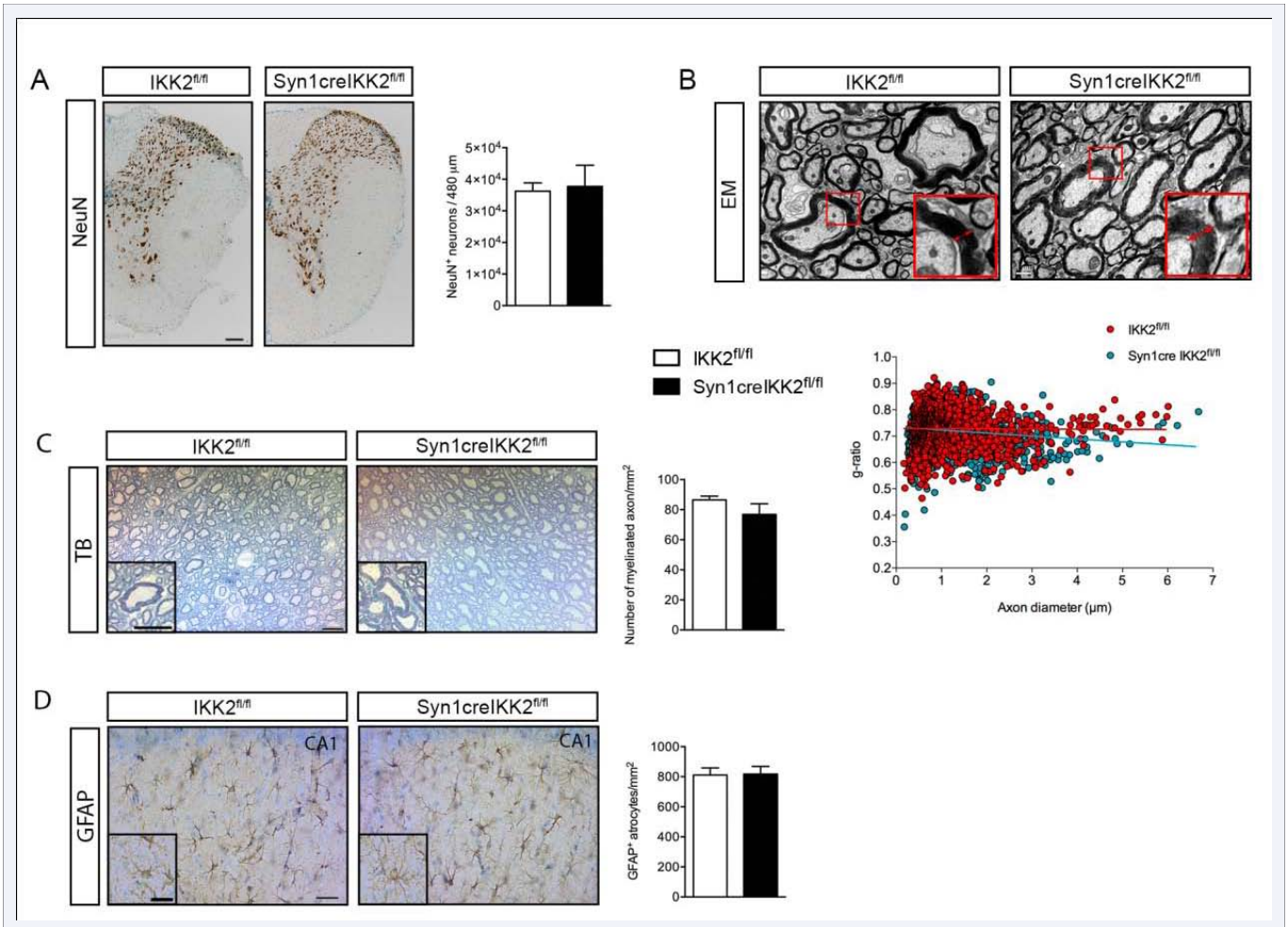

Figure 1 The impact of conditional ablation of neuronal IKK2 on neurons, axons and astrocytes. (A) Photomicrographs of NeuN^{+} neurons located in the thoracic part of the spinal cord in naïve IKK2$^{fl/fl}$ and Syn1CreIKK2$^{fl/fl}$ mice. Scale bar=100µm. The number of NeuN^{+} neurons/480µm was comparable between genotypes (student's t-test), n=3 mice/group. (**B**) Representative electron micrographs of lateral columns of the thoracic spinal cord comparing naïve IKK2$^{fl/fl}$ and Syn1creIKK2$^{fl/fl}$ mice. Red arrows show the average thickness of the myelin sheets in representative myelinated axons. Scale bar=1µm. Representation of the g-ratio vs. the corresponding axon diameter in naïve conditions (scatter plot), n=5 mice/group. (**C**) Representative photomicrographs of toluidine blue stained ultrathin sections of the thoracic spinal cord of naïve IKK2$^{fl/fl}$ and Syn1creIKK2$^{fl/fl}$ mice. Scale bars=50m. Quantification of toluidine blue-stained myelinated axons showed comparable numbers of myelinated axons/mm^2 between IKK2$^{fl/fl}$ and Syn1creIKK2$^{fl/fl}$ mice (student's t-test), n=5 mice/group. (**D**) Representative photomicrographs of hippocampal GFAP^{+} astrocytes from IKK2$^{fl/fl}$ and Syn1creIKK2$^{fl/fl}$ mice. Scale bars=40µm, insert 30µm. Quantification of the number of GFAP^{+} astrocytes/mm^2 showed comparable numbers of astrocytes between IKK2$^{fl/fl}$ and Syn1creIKK2$^{fl/fl}$ mice (student's t-test), n=7-8 mice/group. All data are presented as mean±SEM.

in number of neurons in the spinal cord under naïve conditions (Figure 1A). Evaluation of myelin thickness by measurement of the g-ratio (Figure 1B) showed no difference except for axons <1.5-2.0 µm, where the g-ratio was mildly reduced ($p<0.05$), which could be reflective of more compact myelin. We plotted the g-ratio against the corresponding axon diameter and found by linear regression analysis that the slopes differed significantly ($Syn1creIKK2^{fl/fl}$ = 0.734 ± 0.002 vs $IKK2^{fl/fl}$ = 0.729 ± 0.002, $p<0.0001$, student's t-test) (Fig. 1B, scatter plot). $Syn1creIKK2^{fl/fl}$ mice showed lower g-ratios than littermates with increasing axon diameter, shown by reduced elevation of the linear regression with increasing axon diameters. Because the slopes differed so much, it was not possible to test whether the intercepts differed significantly. However, the total number of myelinated axons/mm^2 was comparable between $IKK2^{fl/fl}$ and $Syn1creIKK2^{fl/fl}$ mice (Figure 1C). Also, the total number of $GFAP^+$ astrocytes/mm^2 in the hippocampus was comparable between $Syn1creIKK2^{fl/fl}$ mice and littermates (Figure 1D).

Memory retention is impaired in $Syn1creIKK2^{fl/fl}$ mice

In order to investigate whether neuronal ablation of IKK2 was associated with any alterations in learning and memory, we performed the Barnes maze test. We found that $IKK2^{fl/fl}$ and $Syn1creIKK2^{fl/fl}$ mice performed similarly during the habituation phase and training trials demonstrating similar abilities to learn where the hidden goal box was placed (Figure 2A). No differences in learning abilities between the two genotypes were found (Figure 2B). On the probe day (day 5), when the goal box was removed, $IKK2^{fl/fl}$ mice spent significantly less time in the target quadrant during the last two trials compared to the first trial and significantly less time in the opposite quadrant during the first four trials compared to the last trial, suggesting that memory retention was intact in $IKK2^{fl/fl}$ mice. $Syn1creIKK2^{fl/fl}$ mice did not significantly change the time spent in the target or opposite

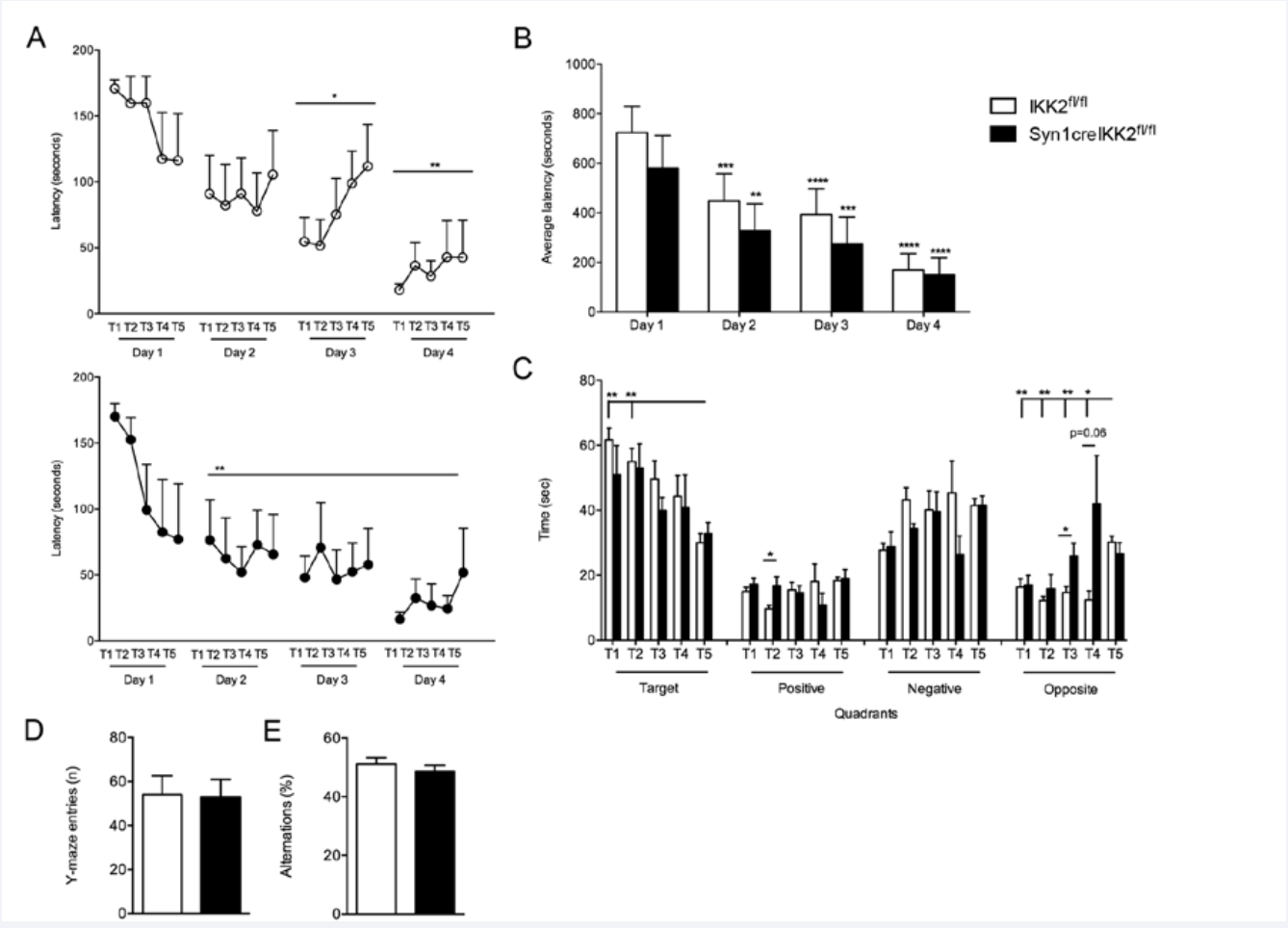

Figure 2 Neuronal ablation of IKK2 affects memory retention under naïve conditions. (A) Primary latency of habituation and training trails in the Barnes maze test. $IKK2^{fl/fl}$ and $Syn1creIKK2^{fl/fl}$ mice both decreased their latency time to find the hidden goal box over the 4 trial days with 5 trials each day (T1-5) (one-way RM ANOVA, Tukey's *post hoc*) (**B**) Comparison of average latency times to find the hidden goal box between $IKK2^{fl/fl}$ and $Syn1creIKK2^{fl/fl}$ mice. Both genotypes decreased their average latency time to find the hidden goal box (two-way RM ANOVA time $F_{3,27}$ = 37.63; genotype $F_{1,9}$ = 0.55; time:genotype $F_{3,27}$ = 0.70, followed by Tukey's *post hoc*), with no difference between genotypes. (**C**) Total time searched for the hidden goal box, on probe day, in each of the four quadrants as a measure of memory retention. $Syn1creIKK2^{fl/fl}$ mice displayed impaired memory retention (5 trials on probe day, T1-5) (one-way RM ANOVA, followed by Tukey's *post hoc*). (**D**, **E**) Total number of Y-maze entries (**D**) and spontaneous alternation behavior (%) (**E**) Under naïve conditions. No difference was observed between genotypes. n=6 mice/group. All data are presented as mean±SEM. *p<0.05, **p<0.01, ***p<0.001, ****p<0.0001.

quadrant (Figure 2C), suggesting that memory retention was impaired in Syn1creIKK2$^{fl/fl}$ mice.

To test whether short-term memory was affected, we used the Y-maze test (Figure 2D,E). We found no differences in the total number of Y maze entries (Figure 2D) or in alternation behavior (Figure 2E) between the two genotypes, suggesting that short-term memory is not affected in Syn1creIKK2$^{fl/fl}$ mice.

Syn1CreIKK2$^{fl/fl}$ mice display impaired motor function under naïve conditions

Next, we tested for changes in loco motor function and anxiety-related behavior under naïve conditions. The rotarod performance test was used to evaluate endurance, balance and motor coordination (Figure 3A, B). Both IKK2$^{fl/fl}$ and Syn1creIKK2$^{fl/fl}$ mice were capable of learning how to walk on the rotarod (T1-T4), however motor function was significantly impaired in Syn1creIKK2$^{fl/fl}$ mice compared to IKK2$^{fl/fl}$ mice, since they spent significantly less time on the rotarod, both during each trial (Figure 3A) and in total (Figure 3B). Nociception was tested using the Hargreave's test for thermal hyperalgesia. No difference was found in the latency to remove the paws between IKK2$^{fl/fl}$ and Syn1creIKK2$^{fl/fl}$ mice (Figure 3C). Also, no difference was observed in neuromuscular function, since the strength was comparable between the two genotypes (Figure 3D). Finally, the mice were tested for anxiety-related behavior and locomotion using the EPM (Figure 3E-G) and the open field tests (Figure 3H-K). In the EPM, we found no difference in the time spent in the open arm (Figure 3E), closed arm (Figure 3F), or in the total distance travelled (Figure 3G). However, in the open field test, we found

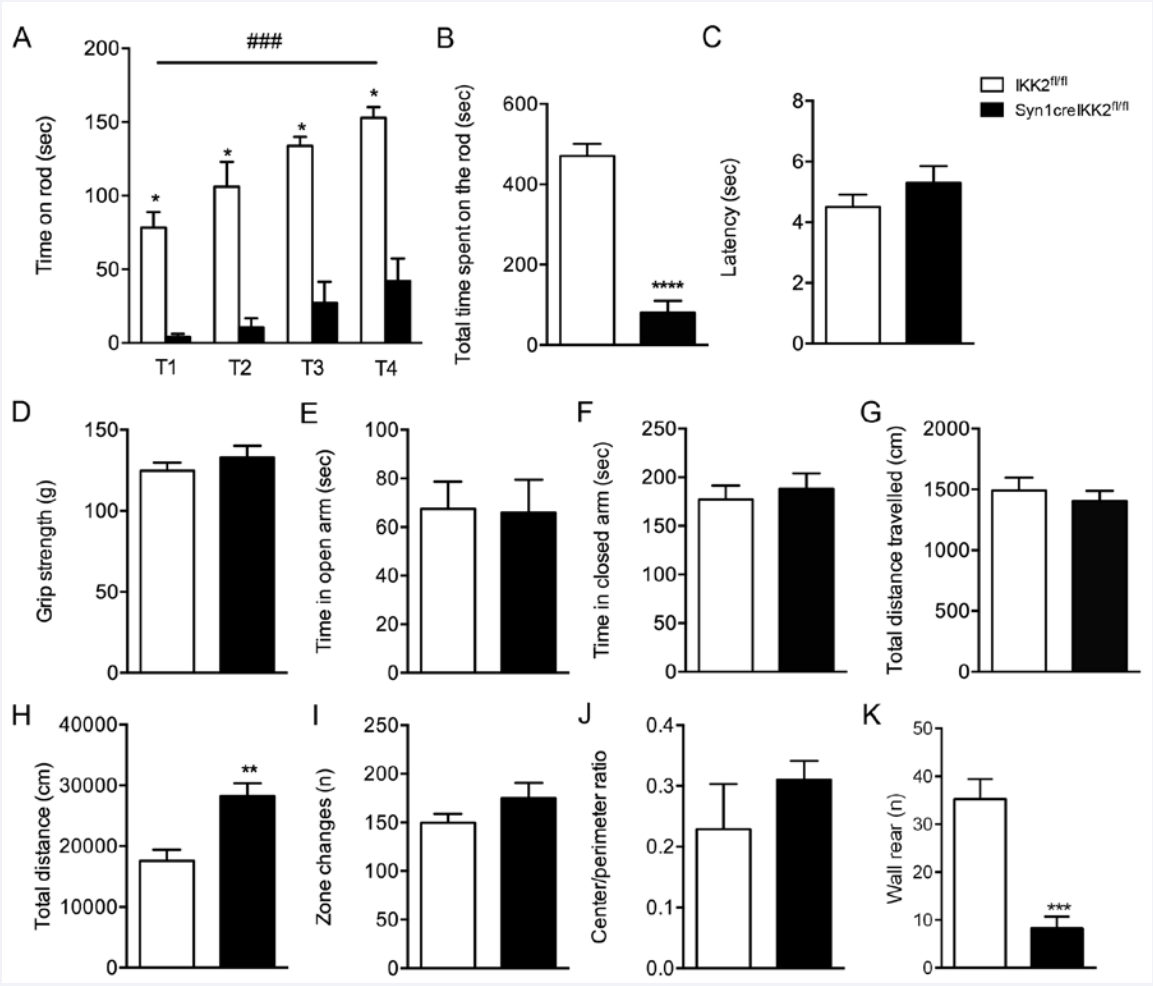

Figure 3 Baseline behavioral analysis of naïve Syn1creIKK2$^{fl/fl}$ and IKK2$^{fl/fl}$ mice. (**A**, **B**) Rotarod performance under naïve conditions. A learning component is observed in both genotypes (two-way RM ANOVA), but Syn1creIKK2$^{fl/fl}$ mice spent significantly less time on the rod than littermates during each trial (T1-4) (two-way ANOVA, *post hoc* multiple t-test) (**A**) and in total (student's t-test) (**B**) demonstrating impaired motor coordination (n=6 mice/group). (**C**) Hargreaves test showing comparable latency to remove paws between IKK2$^{fl/fl}$ and Syn1creIKK2$^{fl/fl}$ mice under naïve conditions (n=6 mice/group). (**D**) Grip strength (g, gram) analysis showed comparable neuromuscular function in naïve IKK2$^{fl/fl}$ and Syn1creIKK2$^{fl/fl}$ mice (n=16 mice/group). (**E-G**) Elevated plus maze test showed that IKK2$^{fl/fl}$ and Syn1creIKK2$^{fl/fl}$ mice spent comparable amounts of time in the open (**E**) and closed (**F**) arms and travelled a similar total distance during the trial (**G**) (n=12-13 mice/group). (**I-K**) Open field test showed that Syn1creIKK2$^{fl/fl}$ mice travelled a significantly longer distance than IKK2$^{fl/fl}$ mice in the open field (student's t-test) (**H**), whereas number of zone changes (**I**), center/perimeter ratio (**J**)were comparable between genotypes,and number of wall rearing (**K**) was significantly decreased for Syn1creIKK2$^{fl/fl}$ mice compared to IKK2$^{fl/fl}$ mice, n=6 mice/group. All data are presented as mean±SEM. *p<0.05, **p<0.01, ###p<0.001 ****p<0.0001.

that Syn1creIKK2$^{fl/fl}$ mice travelled a significantly longer distance (Figure 3H) and displayed increased wall rearing compared to littermates (Figure 3K). No differences were observed in number of zone changes (Figure 3I), center/perimeter ratio (Figure 3J), latency to first rear, grooming, center rear, urination, droppings, diggings or latency to first rear (Table 1).

Neuronal IKK2 ablation improves the functional outcome after SCI

Following moderate contusive SCI, both IKK2$^{fl/fl}$ and Syn1CreIKK2$^{fl/fl}$ mice showed improvement in the loco motor behavior. BMS scores were significantly different between the two genotypes at day 21 and 35, with IKK2$^{fl/fl}$ mice performing worse than Syn1creIKK2$^{fl/fl}$ (Figure 4A). BMS subscores were significantly reduced in IKK2$^{fl/fl}$ mice at day 14, 21, 28 and 35, compared to Syn1creIKK2$^{fl/fl}$ mice (Figure 4B). Using the rung walk test, we found that both groups significantly increased the number of miss steps after SCI compared but with no differences between genotypes (Figure 4C). At day 28 and 35 after SCI, both IKK2$^{fl/fl}$ and Syn1creIKK2$^{fl/fl}$ decreased the number of missteps compared to 21 days after SCI (Figure 4C). No differences were observed in latency to remove paws in the Hargreave's test, even

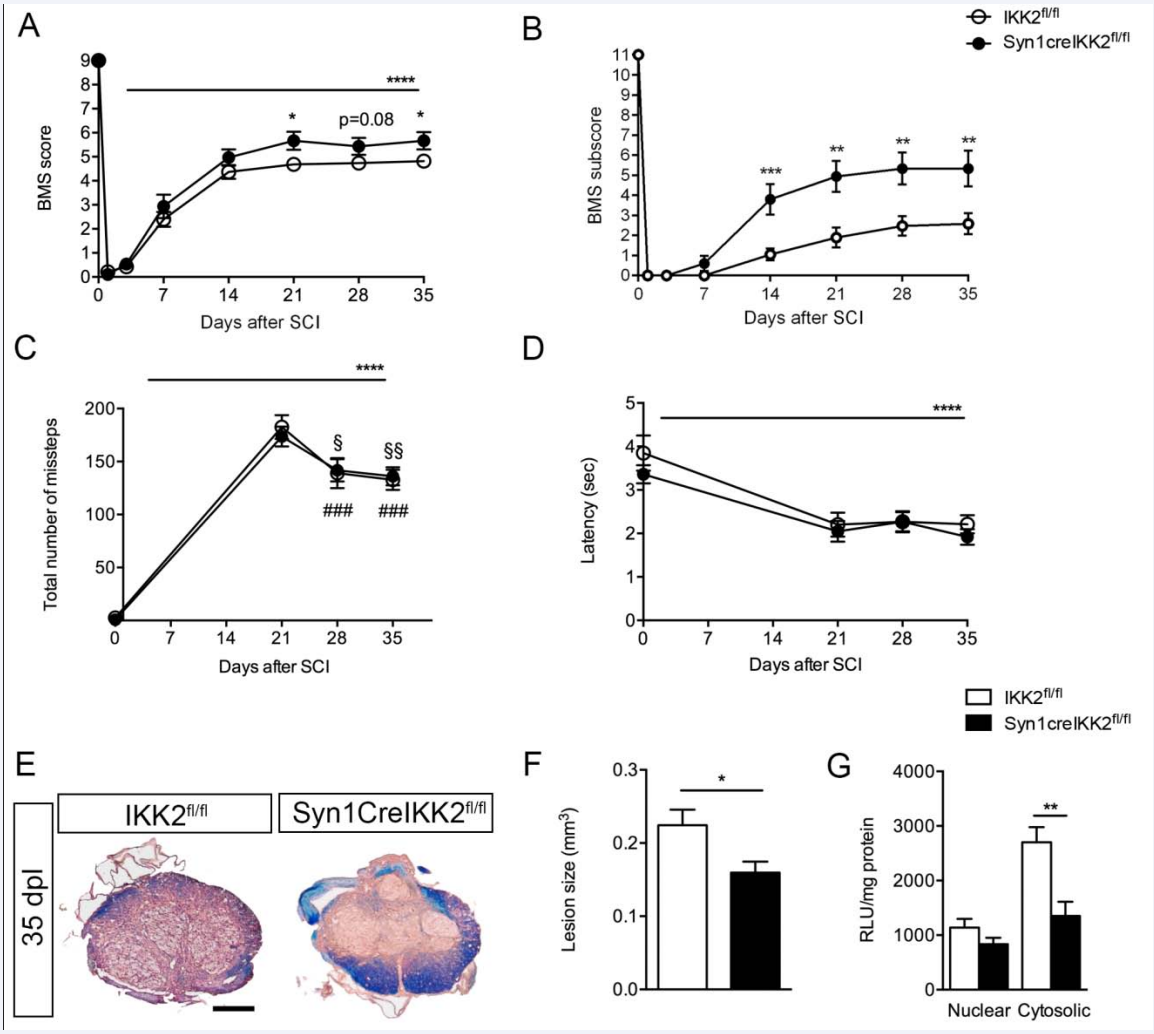

Figure 4 Neuronal ablation of IKK2 improves functional outcome and decreases lesion size after SCI. (**A**) Analysis of BMS scores in IKK2$^{fl/fl}$ and Syn1creIKK2$^{fl/fl}$ mice 35 days after SCI showed that conditional ablation of IKK2 in neurons significantly improved BMS after SCI (two-way ANOVA, *post hoc* multiple t-test). Both groups of mice significantly improved their BMS score over time (two-way RM ANOVA $F_{7,224} = 465.9$). (**B**) Analysis of BMS subscore in IKK2$^{fl/fl}$ and Syn1creIKK2$^{fl/fl}$ mice 35 days after SCI showed that conditional ablation of IKK2 in neurons significantly improved BMS (two-way ANOVA, *post hoc* multiple t-test) (**C**) Rung walk analysis showed that both groups of mice increased their number of mistakes after SCI (two-way RM ANOVA, ****p<0.0001, time $F_{3,57} = 213.5$, followed by Tukey's *post hoc*), n=10-11 mice/group, no differences between genotypes were observed. Both genotypes decreased the number of mistakes on the rung walk at day 28 and 35 compared to day 21 (Syn1creIKK2$^{fl/fl}$: §<0.05, §§<0.01, and IKK2$^{fl/fl}$: ###p<0.001). (**D**) Thermal stimulation using the Hargreave's test showed no differences in latency time to withdraw paws between genotypes. Both groups decreased latency to remove their hind paws over time after SCI (two-way RM ANOVA, time $F_{3,54} = 19.87$), n=10 mice/group. (**E**) Representative luxol fast blue (LFB) stained thoracic spinal cord sections from IKK2$^{fl/fl}$ and Syn1creIKK2$^{fl/fl}$ miceallowed 35 days survival after SCI. Scale bar=200µm. (**F**) Analysis of lesion volumes in LFB stained sections 35 days after SCI showed that conditional ablation of neuronal IKK2 significantly decreased lesion size(student's t-test), n=6-7 mice/group. (**G**) Quantitative analysis of cytoplasmic and nuclear phosphorylated NF-κB (ser536) 3 days after SCI, n=5 mice/group. All results are expressed as mean±SEM. *p<0.05, **p<0.01, ***p<0.001, ****p<0.0001.

though both groups of mice significantly decreased latency times following SCI (Figure 4D). Lesion volume analysis at 35 days after SCI (Figure 4E) showed that lesion size was significantly decreased in Syn1creIKK2$^{fl/fl}$ mice compared to littermates (Figure 4F). Together these data indicate that ablation of neuronal IKK2 is protective following SCI (Table 2).

Conditional ablation of IKK2 in neurons reduces cytosolic phospho-NF-κB

We observed a decrease in NF-κB activation, measured by probing for cytoplasmic phospho-NF-κB, 3 days after SCI in Syn1creIKK2$^{fl/fl}$ compared to littermates (Figure 4G), demonstrating successful ablation of IKK2 in our Syn1creIKK2$^{fl/fl}$ mice. We observed no significant difference in nuclear phospho-NF-κB (Figure 4G) or in non-injured mice (data not shown).

Conditional deletion of neuronal IKK2 decreases IL-1β 3 days after SCI

In order to investigate whether decreased cytoplasmic phospho-NF-κB resulted in an altered inflammatory response within the lesioned spinal cord, we performed protein analysis for a number of inflammatory cytokines (Figure 5). We found that IL-1β was increased in both genotypes 3 days after SCI (Figure 5A), but to a significant lower extent in Syn1creIKK2$^{fl/fl}$ mice (Figure 5A). Also IL-1Ra increased significantly 3 days after SCI in both IKK2$^{fl/fl}$ and Syn1creIKK2$^{fl/fl}$ mice, but no difference was observed between genotypes (Figure 5B). We found a significant correlation between IL-1β and IL-1Ra 3 days after SCI (Figure 5C) and IL-1β/IL-1Ra ratios were found to be 1:17 in naïve IKK2$^{fl/fl}$, 1:20 in naïve Syn1creIKK2$^{fl/fl}$ mice, and 1:19 and 1:21, respectively 3 days after SCI. TNF (Figure 5D), IL-6 (Figure 5E), IL-10 (Figure 5F), IL-5 (Figure 5G) and CXCL1 (Figure 5H) were all up regulated 3 days after SCI, but with no differences between genotypes. At 3 days, IL-10 and TNF levels (Figure 5I) and IL-10 and CXCL1 levels (Figure 5J) were found to correlate significantly.

Microglial/leukocyte F4/80 and CD45 expression is comparable between IKK2$^{fl/fl}$ and Syn1creIKK2$^{fl/fl}$ mice 35 days after SCI

Microscopic evaluation of F4/80^{+} (Figure 6A) and CD45^{+} (Figure 6B) microglial/leukocyte activation patterns revealed that cells located near the epicenter displayed a macrophage-like morphology with large round cell bodies, whereas F4/80^{+} and CD45^{+} cells located further away from the epicenter displayed a more microglial-like morphology with small cell bodies and numerous branched processes, similarly to what we have previously observed at this time point [24]. No difference in the distribution or the density of the cells was observed between IKK2$^{fl/fl}$ and Syn1creIKK2$^{fl/fl}$ mice.

DISCUSSION

As consolidation of explicit long-term memory requires a series of hippocampus-dependent molecular processes, including gene transcription, and NF-κB, which consists of p50, p65 and c-Rel subunits [10], is known to be specifically involved in the regulation of neuronal plasticity and memory formation [31,32], we tested Syn1creIKK2$^{fl/fl}$ mice for memory deficits and found impairment in memory consolidation. This is in line with previous findings demonstrating involvement of NF-κB in long-term synaptic plasticity and memory formation [33-38]. p50$^{-/-}$ mice exhibit learning deficits in the active avoidance test [35], but enhanced learning in aversive tests, such as the water maze test, and increased levels of basal anxiety in the open field and

Table 1: Baseline behavior in naïve IKK2$^{fl/fl}$ and Syn1creIKK2$^{fl/fl}$ mice.

Open Field test	IKK2$^{fl/fl}$ (n = 6)	Syn1creIKK2$^{fl/fl}$ (n = 6)	*p*-value
Grooming	4.67 ± 1.05	3.67 ± 0.92	0.49
Center rear	7.33 ± 3.69	16.17 ± 4.42	0.16
Urination	0.17 ± 0.17	0.67 ± 0.33	0.21
Droppings	4.00 ± 2.19	3.00 ± 0.26	0.31
Diggings	2.17 ± 0.75	3.17 ± 4.26	0.61
Time of first rear	59.20 ± 34.13	28.12 ± 3,84	0.39

Data are presented as mean number of events ± SEM. Student's t-test. ****p<0.0001

Table 2: Open field test 35 days after SCI in IKK2$^{fl/fl}$ and Syn1creIKK2$^{fl/fl}$ mice.

Open Field test	IKK2$^{fl/fl}$ (n = 4-7)	Syn1creIKK2$^{fl/fl}$ (n = 9)	p-value
Total distance (cm)	3,531 ± 125.2	4,624 ± 656.1	0.30
Total entries (n)	32.0 ± 6.8	22.6 ± 6.0	0.37
Total resting time (sec)	83.9 ± 13.4	71.1 ± 12.5	0.55
Center/perimeter ratio	0.054 ± 0.013	0.027 ± 0.008	0.09
Grooming	1.43 ± 0.30	2.00 ± 0.44	0.33
Droppings	2.00 ± 0.31	1.44 ± 0.38	0.29
Urination	0.86 ± 0.40	0.89 ± 0.35	0.95

Data are presented as mean ± SEM. Student's t-test.

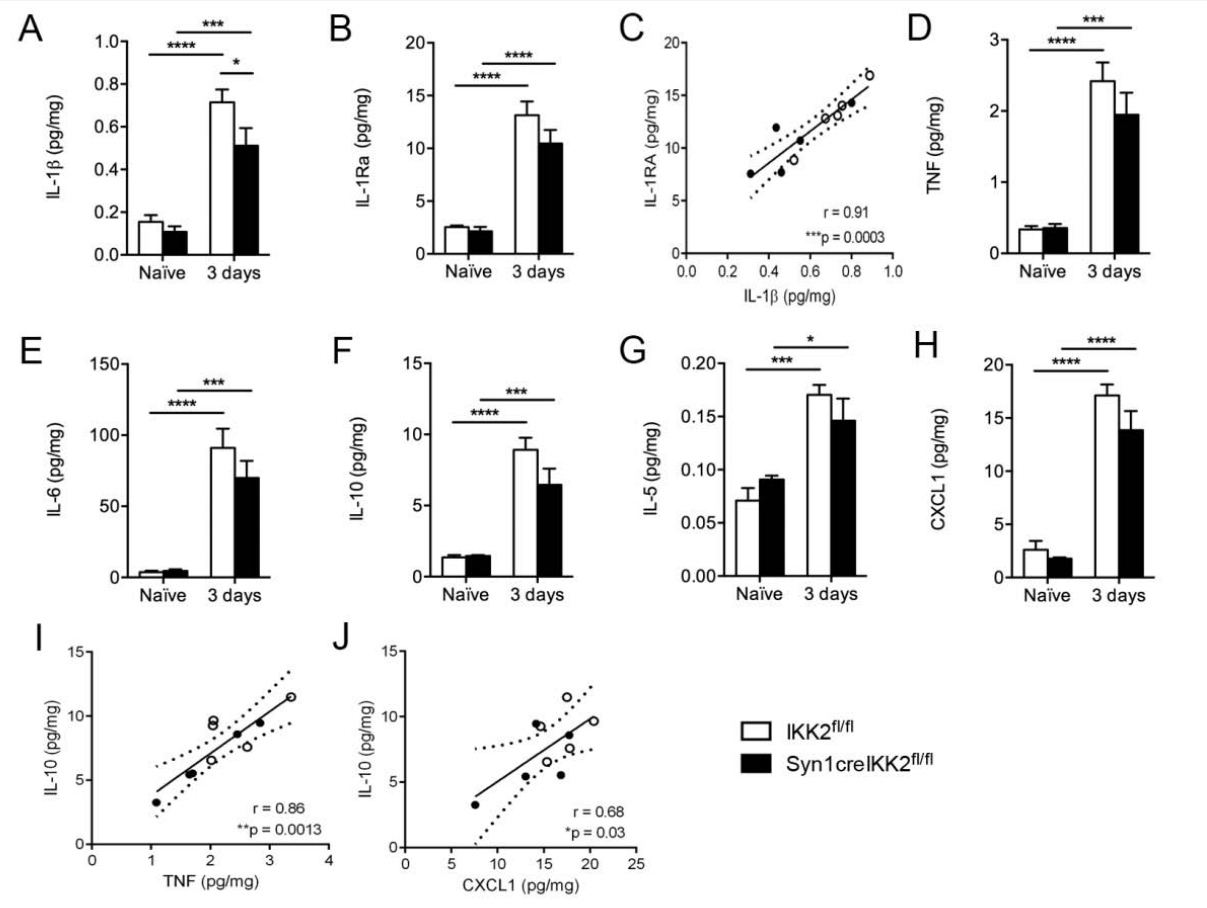

Figure 5 Cytokine expression profiling after SCI. (**A-K**) IL-1β (time: $F_{1,16}$ = 77.88; genotype $F_{1,16}$ = 5.16; time: genotype $F_{1,16}$ = 2.06) (**A**), IL-1Ra (time: $F_{1,15}$= 90.23) (**B**), IL-1β versus IL-1Ra correlation 3 days after SCI (**C**), TNF (time: $F_{1,16}$ = 78.79) (**D**), IL-6 (time: $F_{1,16}$ = 70.66) (**E**), IL-10 (time: $F_{1,16}$ = 77.15) (**F**), IL-5 (time: $F_{1,16}$ = 35.55) (**G**), and CXCL1 (time: $F_{1,16}$ = 143.0) (**H**) protein levels were quantified in naïve conditions and 3 days after SCI in $IKK2^{fl/fl}$ and $Syn1creIKK2^{fl/fl}$ mice. For each protein, results are expressed as mean±SEM, n=5mice/group (two-way ANOVA with Bonferroni *post hoc* test). *p<0.05, ***p<0.001 and ****p<0.0001. (**I**,**J**) Correlation analyses of IL-10 versus TNF (**I**) and IL-10 versus CXCL1 (**J**) 3 days after SCI. *p<0.05, **p<0.01, ***p<0.001, Pearson correlation test. Data are normalized to α-actin protein expression n=4 mice/group (two-way ANOVA with Bonferroni *post hoc* test). **p<0.01.

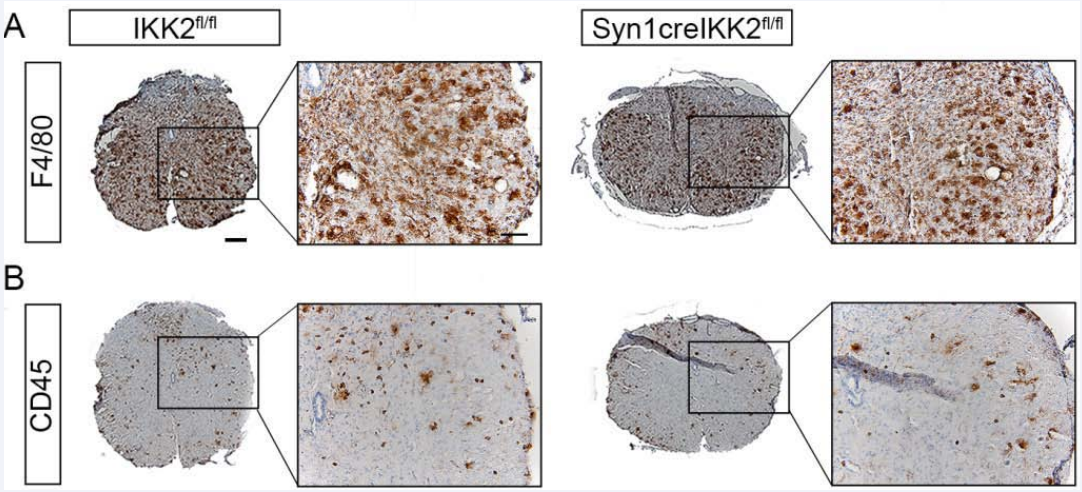

Figure 6 Microglial and leukocyte immunoreactivity 35 days after SCI. (**A**,**B**) Immunohistochemical staining for F4/80 (**A**) and CD45 (**B**) were comparable between $IKK2^{fl/fl}$ and $Syn1creIKK2^{fl/fl}$ mice 35 days after SCI. Analysis was based on 5 sections from each animal, n=5 mice/group. Scale bars: low magnification = 200μm and high magnification = 100μm.

light/dark box tests, all of which seemed to be accompanied by activation of the stress (hypothalamic-pituitary-adrenal) axis and increased corticosterone levels [36]. In the Barnes maze test, spatial learning was not affected in $p50^{-/-}$ mice [36], whereas, mice with deleted p65 gene and simultaneous ablation of TNFR1 ($TNFR^{-/-}p65^{-/-}$) display spatial learning deficits in the radial arm maze [34] and c-$Rel^{-/-}$ mice also display impaired hippocampus-dependent memory formation using the novel recognition test [39]. The finding, that conditional ablation of IKK2 in neurons lead to impaired memory retention in $Syn1creIKK2^{fl/fl}$ mice suggests that the neuronal, classical NF-B pathway is important for memory retention in naïve conditions.

Previous studies have indicated NF-κB as an important regulator of energy metabolism, as $p50^{-/-}$ mice showed significantly longer total running time on the rotarod and an anti-obesity phenotype compared to control mice [40]. This is in contrast to findings in the present study, as we observed increased body weight and an impaired motor function phenotype in the rotarod test in our $Syn1creIKK2^{fl/fl}$ mice. Targeted ablation of IKK2 in muscle creatine kinase^{+} cells leads to improved muscle strength and appears to be an important modulator of muscle homeostasis [30], whereas targeted ablation of IKK2 in neurons in the present study was not associated with altered skeletal muscle strength, as assessed by the grip strength test.

The Synapsin 1 promoter driven cre expression has previously been shown to be effective in ablating neuronal genes for studying specific functions of neurons [16,41]. In the present study, we observed a significant decrease in phospho-NF-κB in the cytosplasmic cell compartment of $Syn1creIKK2^{fl/fl}$ mice 3 days after SCI compared to littermates, suggesting that we also achieved efficient ablation of IKK2 in neurons. Neuronal cytoplasmic p65 levels are known to peak at later time points (after 24 hours) than neuronal nuclear p65 levels (6 hours) [4], which may explain why we only observed a significant increase in cytoplasmic and not in nuclear phospho-NF-κB levels. The decrease in cytoplasmic phospho-NF-κB (ser536) in $Syn1creIKK2^{fl/fl}$ compared to $IKK2^{fl/fl}$ mice 3 days after SCI is consistent with expectation that neuronal ablation of IKK2 decreases NF-κB activation after SCI, and validates the use of this mouse model.

The decrease in NF-κB activation in the $Syn1creIKK2^{fl/fl}$ mice subsequently lead to improved functional recovery and reduced lesion size 35 days after SCI. These findings are in accordance with previous suggestions that IKK inhibitors may be useful in the therapy of SCI [8, 42]. The IKK2 selective inhibitor BMS-345541 (4-(2'-aminoethyl) amino-1,8-dimethylimidazol(1,2-a) quinoxaline) [8] and butein (3,4,2',4'-tetrahydroxychalcone), and IKK/NF-κB inhibitor [42], have been shown to be protective in rats after SCI by reducing the infiltration of neutrophils and by inhibiting caspase-3 activation. Furthermore, in $LysMcreIKK2^{fl/fl}$ mice, conditional ablation of myeloid IKK2 resulted in decreased CXCL1 expression, decreased neutrophil and macrophage infiltration, decreased pro-inflammatory gene expression (IL-6, IL-1β, TNF, iNOS, and COX2) and neuronal cell death and improved BMS score compared to $IKK2^{+/+}$ wild type mice [43]. In the present study, we did not observe any changes in CXCL1, a chemokine known to preferentially attract neutrophils, between $IKK2^{fl/fl}$ and $Syn1creIKK2^{fl/fl}$ mice after SCI. We also did not observe any apparent differences in microglial/leukocyte responses between genotypes 35 days after SCI. However, we did find significant differences in IL-1β expression within the lesioned cord, with levels being significantly decreased in $Syn1creIKK2^{fl/fl}$ compared to littermates 3 days after SCI. IL-1β is known to induce a prolonged stimulation of NF-κB/Rel factors by inducing both IB and IB degradation and by activating the NF-κB p50, p65 and c-Rel subunits, of which the p65 is involved glutamate-mediated cell death and c-Rel in IL-1β-preserved cell survival [44]. In addition, the heterodimeric p65/p50 NF-κB protein complex selectively binds inflammatory gene promoter sites, resulting in especially increased IL-1β levels, which can be antagonized by administration of IL-1 receptor antagonist (IL-1Ra) [44,45]. It is therefore possible that decreased neuronal IKK2 results in decreased NF-κB activation, followed by decreased transcription of the IL-1 gene and a subsequent decrease in IL-1β expression. An imbalance between IL-1 (IL-1β + IL-1α) and IL-1Ra, which is a neuroprotective anti-inflammatory cytokine [28], has been shown to determine the degree of cardiac remodeling after myocardial infarction [46], and a high IL-1RA/IL-1β ratio is associated with a better outcome in patients after traumatic brain injury [47] and in mice after experimental stroke [28]. In the present study, we did, however, not observe any difference in IL-1Ra, which could account for the neuroprotection we observed after SCI in our $Syn1creIKK2^{fl/fl}$ mice. In addition, the IL-1RA/IL-1β ratios were comparable between genotypes. However, as intracellular IL-1Ra could regulate the action of intracellular IL-1α[48], it is possible that also IL-1α levels are decreased in our $Syn1creIKK2^{fl/fl}$ mice shifting the IL-1Ra/IL-1 towards neuroprotection.

AsIL-1 stimulation of NF-κB activity also stimulates transcription of iNOS [49], it is possible that conditional ablation of neuronal IKK2 may have caused a decrease in iNOS levels followed by subsequent decrease in reactive oxygen species and neuroprotection. Indeed, iNOS immunoreactivity has been detected in neurons following SCI [49] and inhibition of NF-κB activation using pyrrolidine dithiocarbamate has been shown to attenuate inflammation and oxidative stress following SCI in rats [50].

NF-κB is constitutively activated in neurons of the developing and, at least in part, of the mature CNS [51].There is accumulating evidence that p65 is crucial for axon formation during embryonic neural development [52] and that p65 and p50 can either promote or inhibit axogenesis during postnatal development [53,54].Indeed, cell-type specific deletion of p65 in neurons and/or microglia has been shown to stimulate axonal regeneration after axonal injury in adult mice [55]. It is possible that conditional ablation of neuronal IKK2 leads to a functional shift from neurite-inhibiting to neurite-promoting signaling in our $Syn1creIKK2^{fl/fl}$ mice resulting in increased axoneogenesis and improved functional outcome 35 days after SCI. A rationale for this positive effect of inhibiting the canonical NF-κB signaling is its activation in transected nerve fibers and associated cell soma, as activated NF-κB may trigger a cell death program inside axotomized neurons [56]. As functional recovery following SCI ideally relies on the presence of a large number of surviving neurons, reducing cell death by diminished activation of NF-κB is an advantage for promoting axonal regeneration and network

restoration. It remains to be explored whether axoneogenesis is improved following SCI in our Syn1creIKK2$^{fl/fl}$ mice.

CONCLUSION

We conclude that NF-κB-dependent processes initiated in neurons are important for the development of damage after SCI and that inhibition of such processes by conditional ablation of neuronal IKK2 leads to functional improvement after SCI. Given the very few pharmacological tools available, our study identifies a new potential target for development of treatments for SCI. We are aware that NF-κB is an important ubiquitous molecule necessary for a variety of vital functions, including inhibition of apoptotic cell death [57], and as such inhibiting NF-κB may cause serious side effects. However, inhibiting NF-κB activation at the very early time points after SCI, where maximal NF-κB is observed [1], may prevent subsequent activation of deleterious inflammatory cascades, thereby favoring an environment more suitable for axonal preservation and functional recovery.

ACKNOWLEDGEMENTS

DGE and KLL conceived the studies, designed experiments, performed statistical analysis and wrote the paper. DGE, HGN, LHJ, MCL, MY-K, PMM, JHV, SD, JRB, KL-H, RB performed experiments, analyzed and interpreted data. All authors read and approved the final manuscript.

We thank Dr. Michael Karin for originally donating the IKK2$^{fl/fl}$ mice to Professor John Bethea at the Miami Project to Cure Paralysis, University of Miami Miller School of Medicine, where these studies were initiated. Shaffiat Karmally, Louise Lykkemark Christensen, Dorte Lyholmer and Signe Marie Andersen are acknowledged for skillful technical assistance. We are grateful to Margaret Bates and Vania Almeida at the Electron Microscopy Core Facility of The Miami Project to Cure Paralysis for their technical assistance in all aspects of EM imaging and TB staining. This study was supported by the International Foundation for Research in Paraplegia (P128) (KLL), the Danish Association for Paraplegics – RYK and Claus Madsen's Foundation (KLL), the Carlsberg Foundation (2007_01_0176) (KLL), Simon Fougner Hartmanns Familiefond (KLL), Pumpkin-Aarhus University (KLL and KL-H), Overlægerådets Forskningsfond – Odense University Hospital (DGE), Fondentil Lægevidenskabens Fremme (KLL and DGE), The Søren & Johanne WiibroSegel's Research Fund (DGE), Kong Christian X's Fond (DGE), Institute of Molecular Medicine, SDU (DGE), and the Faculty of Health Science, SDU (DGE), NINDS grants NS084303-01A1 and 1R01NS094522-01 (RB), FISM (Italian Multiple Sclerosis Foundation) grant 2012/R/2 (RB), The Miami Project To Cure Paralysis and the Buoniconti Fund (RB).

REFERENCES

1. Bethea JR, Castro M, Keane RW, Lee TT, Dietrich WD, Yezierski RP. Traumatic spinal cord injury induces nuclear factor-kappaB activation. J Neurosci. 1998; 18: 3251-3260.

2. Brambilla R, Bracchi-Ricard V, Hu WH, Frydel B, Bramwell A, Karmally S, et al. Inhibition of astroglial nuclear factor kappaB reduces inflammation and improves functional recovery after spinal cord injury. J Exp Med. 2005; 202: 145-156.

3. Bracchi-Ricard V, Lambertsen KL, Ricard J, Nathanson L, Karmally S, Johnstone J, et al. Inhibition of astroglial NF-kappaB enhances oligodendrogenesis following spinal cord injury. J Neuroinflammation. 2013; 10: 92.

4. Rafati DS, Geissler K, Johnson K, Unabia G, Hulsebosch C, Nesic-Taylor O, et al. Nuclear factor-kappaB decoy amelioration of spinal cord injury-induced inflammation and behavior outcomes. J Neurosci Res. 2008; 86: 566-580.

5. Brambilla R, Hurtado A, Persaud T, Esham K, Pearse DD, Oudega M, et al. Transgenic inhibition of astroglial NF-kappa B leads to increased axonal sparing and sprouting following spinal cord injury. J Neurochem. 2009; 110: 765-778.

6. Rice T, Larsen J, Rivest S, Yong VW. Characterization of the early neuroinflammation after spinal cord injury in mice. J Neuropathol Exp Neurol. 2007; 66: 184-195.

7. Bastien D, Lacroix S. Cytokine pathways regulating glial and leukocyte function after spinal cord and peripheral nerve injury. Exp Neurol. 2014; 258: 62-77.

8. Han X, Lu M, Wang S, Lv D, Liu H. Targeting IKK/NF-kappaB pathway reduces infiltration of inflammatory cells and apoptosis after spinal cord injury in rats. Neurosci Lett. 2012; 511: 28-32.

9. Brambilla R, Morton PD, Ashbaugh JJ, Karmally S, Lambertsen KL, Bethea JR. Astrocytes play a key role in EAE pathophysiology by orchestrating in the CNS the inflammatory response of resident and peripheral immune cells and by suppressing remyelination. 2014; 62: 452-467.

10. Ghosh S, Karin M. Missing pieces in the NF-kappaB puzzle. Cell. 2002; 109: 81-96.

11. Lawrence T, Bebien M, Liu GY, Nizet V, Karin M. IKKalpha limits macrophage NF-kappaB activation and contributes to the resolution of inflammation. Nature. 2005; 434: 1138-1143.

12. Hilliard B, Samoilova EB, Liu TS, Rostami A, Chen Y. Experimental autoimmune encephalomyelitis in NF-kappa B-deficient mice: roles of NF-kappa B in the activation and differentiation of autoreactive T Cells. J Immunol. 1999; 163: 2937-2943.

13. van Loo G, De Lorenzi R, Schmidt H, Huth M, Mildner A, Schmidt-Supprian M, et al. Inhibition of transcription factor NF-kappaB in the central nervous system ameliorates autoimmune encephalomyelitis in mice. Nature Immunol. 2006; 7: 954-961.

14. Brambilla R, Persaud T, Hu X, Karmally S, Shestopalov VI, Dvoriantchikova G, et al. Transgenic inhibition of astroglial NF-kappa B improves functional outcome in experimental autoimmune encephalomyelitis by suppressing chronic central nervous system inflammation. J Immunol. 2009; 182: 2628-2640.

15. Zhang W, Potrovita I, Tarabin V, Herrmann O, Beer V, Weih F, et al. Neuronal activation of NF-kappaB contributes to cell death in cerebral ischemia. J Cereb Blood Flow Metab. 2005; 25: 30-40.

16. Zhu Y, Romero MI, Ghosh P, Ye Z, Charnay P, Rushing EJ, et al. Ablation of NF1 function in neurons induces abnormal development of cerebral cortex and reactive gliosis in the brain. Genes Dev. 2001; 15: 859-876.

17. Li ZW, Omori SA, Labuda T, Karin M, Rickert RC. IKK beta is required for peripheral B cell survival and proliferation. J Immunol. 2003; 170: 4630-4637.

18. Madsen PM, Clausen BH, Degn M, Thyssen S, Kristensen LK, Svensson M, et al. Genetic ablation of soluble tumor necrosis factor with preservation of membrane tumor necrosis factor is associated with neuroprotection after focal cerebral ischemia. J Cereb Blood Flow Metab. 2016; 36: 1553-1569.

19. Attar A, Liu T, Chan WT, Hayes J, Nejad M, Lei K, et al. A shortened Barnes maze protocol reveals memory deficits at 4-months of age in

the triple-transgenic mouse model of Alzheimer's disease. PLoS One. 2013; 8: 80355.

20. Lambertsen KL, Gramsbergen JB, Sivasaravanaparan M, Ditzel N, Sevelsted-Moller LM, Olivan-Viguera A, et al. Genetic KCa3.1-deficiency produces locomotor hyperactivity and alterations in cerebral monoamine levels. PLoS One. 2012; 7: 47744.

21. Novrup HG, Bracchi-Ricard V, Ellman DG, Ricard J, Jain A, Runko E, et al. Central but not systemic administration of XPro1595 is therapeutic following moderate spinal cord injury in mice. J Neuroinflammation. 2014; 11: 159.

22. Clausen B, Degn M, Martin N, Couch Y, Karimi L, Ormhoj M, et al. Systemically administered anti-TNF therapy ameliorates functional outcomes after focal cerebral ischemia. J Neuroinflammation. 2014; 11: 203.

23. Basso DM, Fisher LC, Anderson AJ, Jakeman LB, Mc Tigue DM, Popovich PG. Basso Mouse Scale for locomotion detects differences in recovery after spinal cord injury in five common mouse strains. J Neurotrauma. 2006; 23: 635-659.

24. Ellman DG, Degn M, Lund MC, Clausen BH, Novrup HG, Flæng SB, et al. Genetic Ablation of Soluble TNF Does Not Affect Lesion Size and Functional Recovery after Moderate Spinal Cord Injury in Mice. Mediators Inflamm. 2016; 2016: 2684098.

25. Jørgensen LH, Sellathurai J, Davis EE, Thedchanamoorthy T, Al-Bader RW, Jensen CH , et al. Delta-like 1 homolog (dlk1): a marker for rhabdomyosarcomas implicated in skeletal muscle regeneration. PLoS One. 2013; 8: 60692.

26. Madsen PM, Motti D, Karmally S, Szymkowski DE, Lambertsen KL, Bethea JR, et al. Oligodendroglial TNFR2 mediates repair in neuroimmune disease by promoting oligodendrocyte differentiation via miRNA modulation. J Neurosci. 2016.

27. Martin NA, Bonner H, Elkjaer ML, D'Orsi B, Chen G, Konig HG, et al. BID Mediates Oxygen-Glucose Deprivation-Induced Neuronal Injury in Organotypic Hippocampal Slice Cultures and Modulates Tissue Inflammation in a Transient Focal Cerebral Ischemia Model without Changing Lesion Volume. Front Cell Neurosci. 2016; 10: 14.

28. Clausen BH, Lambertsen KL, Dagnaes-Hansen F, Babcock AA, von Linstow CU, Meldgaard M, et al. Cell therapy centered on IL-1Ra is neuroprotective in experimental stroke. Acta Neuropathol. 2016.

29. Bradford MM. A rapid and sensitive method for the quantitation of microgram quantities of protein utilizing the principle of protein-dye binding. Analytical biochemistry. 1976; 72: 248-254.

30. Mourkioti F, Kratsios P, Luedde T, Song YH, Delafontaine P, Adami R, et al. Targeted ablation of IKK2 improves skeletal muscle strength, maintains mass, and promotes regeneration. J Clin Invest. 2006; 116: 2945-2954.

31. Meffert MK, Baltimore D. Physiological functions for brain NF-kappaB. Trends Neurosci. 2005; 28: 37-43.

32. Romano A, Freudenthal R, Merlo E, Routtenberg A. Evolutionarily-conserved role of the NF-kappaB transcription factor in neural plasticity and memory. Eur J Neurosci. 2006; 24: 1507-1516.

33. Ahn SY, Cho CH, Park KG, Lee HJ, Lee S, Park SK, et al. Tumor necrosis factor-alpha induces fractalkine expression preferentially in arterial endothelial cells and mithramycin A suppresses TNF-alpha-induced fractalkine expression. Am J Pathol. 2004; 164: 1663-1672.

34. Meffert MK, Chang JM, Wiltgen BJ, Fanselow MS, Baltimore D. NF-kappa B functions in synaptic signaling and behavior. Nat Neurosci. 2003; 6: 1072-1078.

35. Kassed CA, Willing AE, Garbuzova-Davis S, Sanberg PR, Pennypacker KR. Lack of NF-kappaB p50 exacerbates degeneration of hippocampal neurons after chemical exposure and impairs learning. Exp Neurol. 2002; 176: 277-288.

36. Lehmann ML, Brachman RA, Listwak SJ, Herkenham M. NF-kappaB activity affects learning in aversive tasks: possible actions via modulation of the stress axis. Brain Behav Immun. 2010; 24: 1008-1017.

37. O'Mahony A, Raber J, Montano M, Foehr E, Han V, Lu SM, et al. NF-kappaB/Rel regulates inhibitory and excitatory neuronal function and synaptic plasticity. Mol Cell Biol. 2006; 26: 7283-7298.

38. Bracchi-Ricard V, Brambilla R, Levenson J, Hu WH, Bramwell A, Sweatt JD, et al. Astroglial nuclear factor-kappaB regulates learning and memory and synaptic plasticity in female mice. J Neurochem. 2008; 104: 611-623.

39. Ahn HJ, Hernandez CM, Levenson JM, Lubin FD, Liou HC, Sweatt JD. c-Rel, an NF-kappaB family transcription factor, is required for hippocampal long-term synaptic plasticity and memory formation. Learn Mem. 2008; 15: 539-549.

40. Minegishi Y, Haramizu S, Misawa K, Shimotoyodome A, Hase T, Murase T. Deletion of nuclear factor-kappaB p50 upregulates fatty acid utilization and contributes to an anti-obesity and high-endurance phenotype in mice. Am J Physiol Endocrinol Metab. 2015; 309: 523-533.

41. Rempe D, Vangeison G, Hamilton J, Li Y, Jepson M, Federoff HJ. Synapsin I Cre transgene expression in male mice produces germline recombination in progeny. Genesis. 2006; 44: 44-49.

42. Lu M, Wang S, Han X, Lv D. Butein inhibits NF-kappaB activation and reduces infiltration of inflammatory cells and apoptosis after spinal cord injury in rats. Neurosci Lett. 2013; 542: 87-91.

43. Kang J, Jiang MH, Min HJ, Jo EK, Lee S, Karin M, et al. IKK-β-mediated myeloid cell activation exacerbates inflammation and inhibits recovery after spinal cord injury. Eur J Immunol. 2011; 41: 1266-1277.

44. Pizzi M, Goffi F, Boroni F, Benarese M, Perkins SE, Liou HC, et al. Opposing roles for NF-kappa B/Rel factors p65 and c-Rel in the modulation of neuron survival elicited by glutamate and interleukin-1beta. J Biol Chem. 2002; 277: 20717-20723.

45. Hu X, Nesic-Taylor O, Qiu J, Rea HC, Fabian R, Rassin DK, et al. Activation of nuclear factor-kappaB signaling pathway by interleukin-1 after hypoxia/ischemia in neonatal rat hippocampus and cortex. J Neurochem. 2005; 93: 26-37.

46. Abbate A, Salloum FN, Van Tassell BW, Vecile E, Toldo S, Seropian I, et al. Alterations in the interleukin-1/interleukin-1 receptor antagonist balance modulate cardiac remodeling following myocardial infarction in the mouse. PLoS One. 2011; 6: 27923.

47. Hutchinson PJ, O'Connell MT, Rothwell NJ, Hopkins SJ, Nortje J, Carpenter KL, et al. Inflammation in human brain injury: intracerebral concentrations of IL-1alpha, IL-1beta, and their endogenous inhibitor IL-1ra. J Neurotrauma. 2007; 24: 1545-1557.

48. Merhi-Soussi F, Kwak BR, Magne D, Chadjichristos C, Berti M, Pelli G, et al. Interleukin-1 plays a major role in vascular inflammation and atherosclerosis in male apolipoprotein E-knockout mice. Cardiovasc Res. 2005; 66: 583-593.

49. Miscusi M, Ebner F, Ceccariglia S, Menegazzi M, Mariotto S, Berra L, et al. Early nuclear factor-kappaB activation and inducible nitric oxide synthase expression in injured spinal cord neurons correlating with a diffuse reduction of constitutive nitric oxide synthase activity. J Neurosurg Spine. 2006; 4: 485-493.

50. La Rosa G, Cardali S, Genovese T, Conti A, Di Paola R, La Torre D, et al. Inhibition of the nuclear factor-kappaB activation with pyrrolidine

dithiocarbamate attenuating inflammation and oxidative stress after experimental spinal cord trauma in rats. Journal of neurosurgery. 2004; 1: 311-321.

51. Bhakar AL, Tannis LL, Zeindler C, Russo MP, Jobin C, Park DS, et al. Constitutive nuclear factor-kappa B activity is required for central neuron survival. J Neurosci. 2002; 22: 8466-8475.

52. Gavalda N, Gutierrez H, Davies AM. Developmental regulation of sensory neurite growth by the tumor necrosis factor superfamily member LIGHT. J Neurosci. 2009; 29: 1599-1607.

53. Gutierrez H, Davies AM. Regulation of neural process growth, elaboration and structural plasticity by NF-kappaB. Trends Neurosci. 2011; 34: 316-325.

54. Gutierrez H, O'Keeffe GW, Gavaldà N, Gallagher D, Davies AM. Nuclear factor kappa B signaling either stimulates or inhibits neurite growth depending on the phosphorylation status of p65/RelA. J Neurosci. 2008; 28: 8246-8256.

55. Haenold R, Weih F, Herrmann KH, Schmidt KF, Krempler K, Engelmann C, et al. NF-κB controls axonal regeneration and degeneration through cell-specific balance of RelA and p50 in the adult CNS. J Cell Sci. 2014; 127: 3052-3065.

56. Wellmann H, Kaltschmidt B, Kaltschmidt C. Retrograde transport of transcription factor NF-kappa B in living neurons. J Biol Chem. 2001; 276: 11821-11829.

57. Barkett M, Gilmore TD. Control of apoptosis by Rel/NF-kappaB transcription factors. Oncogene. 1999; 18: 6910-6924.

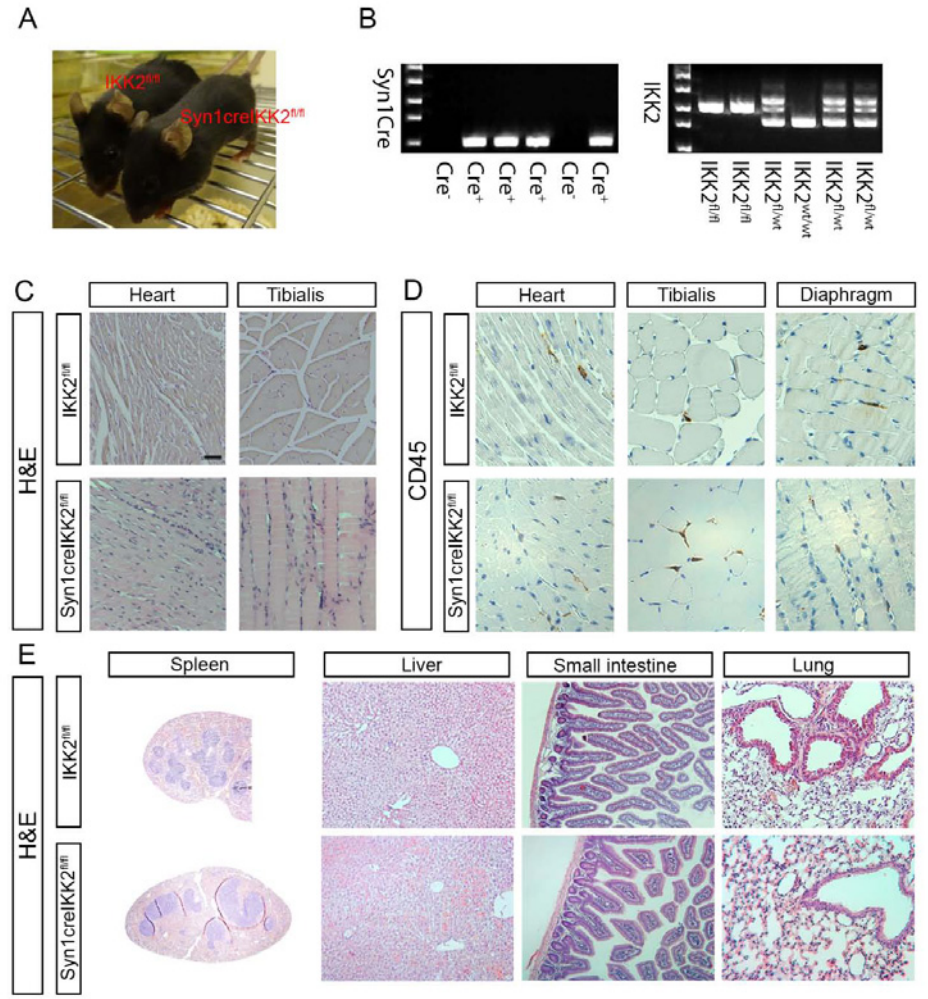

Supplemental Figure 1 Characterization of Syn1creIKK2$^{fl/fl}$ and IKK2$^{fl/fl}$ mice. (**A**) Representative image of female IKK2$^{fl/fl}$ and Syn1creIKK2$^{fl/fl}$ mice. (**B**) RT-PCR analysis of cre (left) and IKK2$^{fl/fl}$ (right) gene expression. (**C**) Representative photomicrographs of haematoxylin and eosin (H&E) stained tissue sections from heart and tibialis musculature showing comparable muscle phenotypes in IKK2$^{fl/fl}$ and Syn1creIKK2$^{fl/fl}$ mice (n=3 mice/group). (**D**) Representative photomicrographs of anti-CD45 stained tissue sections derived from heart, tibialis and diaphragm musculature showing similar muscle phenotypes in IKK2$^{fl/fl}$ and Syn1creIKK2$^{fl/fl}$ mice (n=3 mice/group). (**E**) Representative photomicrographs of H&E stained spleen, liver, small intestine and lung tissue sections from IKK2$^{fl/fl}$ and Syn1creIKK2$^{fl/fl}$ (n=3 mice/group). Scale bars: C, D =40μm; E =200μm for spleen and 40μm for liver, small intestine and lung.

Cite this article

Ellman DG, Novrup HG, Jørgensen LH, Lund MC, Yli-Karjanmaa M, et al. (2017) Neuronal Ablation of IKK2 Decreases Lesion Size and Improves Functional Outcome after Spinal Cord Injury in Mice. JSM Neurosurg Spine 5(2): 1090.